

Article

New Layered Polythiophene-Silica Composite Through the Self-Assembly and Polymerization of Thiophene-Based Silylated Molecular Precursors

Marie-José Zacca, Danielle Laurencin, Sébastien Richeter, Sébastien Clément *  and Ahmad Mehdi * 

Institut Charles Gerhardt, UMR 5253-Université de Montpellier, CNRS, ENSCM-CC1701, Place Eugène Bataillon, F-34095 Montpellier CEDEX 05, France; marie-jose.fadous@hotmail.com (M.-J.Z.); danielle.laurencin@umontpellier.fr (D.L.); sebastien.richeter@umontpellier.fr (S.R.)

* Correspondence: sebastien.clement1@umontpellier.fr (S.C.); ahmad.mehdi@umontpellier.fr (A.M.); Tel.: +33-(0)4-6714-3971 (S.C. & A.M.)

Received: 2 September 2018; Accepted: 28 September 2018; Published: 30 September 2018



Abstract: A new layered hybrid polythiophene-silica material was obtained directly by hydrolysis and polycondensation (sol-gel) of a silylated-thiophene bifunctional precursor, and its subsequent oxidative polymerization by FeCl_3 . This precursor was judiciously designed to guarantee its self-assembly and the formation of a lamellar polymer-silica structure, exploiting the cooperative effect between the hydrogen bonding interactions, originating from the ureido groups and the π -stacking interactions between the thiophene units. The lamellar structure of the polythiophene-silica composite was confirmed by X-ray powder diffraction (XRD) and transmission electron microscopy (TEM) analyses. The solid-state nuclear magnetic resonance (NMR), UV-Vis, and photoluminescence spectra unambiguously indicate the incorporation of polythiophene into the silica matrix. Our work demonstrates that using a polymerizable silylated-thiophene precursor is an efficient approach towards the formation of nanostructured conjugated polymer-based hybrid materials.

Keywords: self-assembly; lamellar; polythiophene; silica; sol-gel; hybrid material

1. Introduction

Conjugated polymers (CPs) have demonstrated a great potential as an active component in a wide range of electronic and optoelectronic devices, such as polymer solar cells [1–3], organic field-effect transistors [4–6], polymer light emitting diodes [7,8], organic batteries [9,10], and biosensors [11,12]. Such devices generally involve complex multi-layered architectures, where the synergistic combination of the CPs and the built-in components determine the intrinsic performance of the devices [13,14]. Indeed, the performances of the devices are intimately related to the interfacial contact between the active layers and the nanoscale morphology of the polymer (which is intrinsically linked to the optoelectronic properties of the polymer) [15–17]. In this respect, controlling the inter-chain interactions, the orientation, and the conformation of the polymer chains are required to minimize the undesirable charge transfer, increase the charge carrier mobilities, and thus, develop devices with enhanced optical and electronic properties [18–20]. CPs are also known to be sensitive to photoinduced oxidation, which affects their electronic and photoconductive properties [21,22].

Incorporation of CPs into an inorganic matrix represents an elegant approach to indirectly control the alignment of polymer chains, to reduce interchain effects by separating the chains and to improve the environmental stability of polymers [23–25]. Consequently, enhanced photoluminescence properties have been achieved through the confinement of polymer chains into nanoporous inorganic

structures [26–29]. A critical issue in the conjugated organic-inorganic hybrid and composite materials lie in the inherent incompatibility between the hydrophilic surface of the metal oxide and the hydrophobic nature of the conjugated polymers, which leads to the aggregation of the conjugated chains, a phenomenon often detrimental to the optical properties [30–32]. To prevent phase separation, intermolecular non-covalent interactions (e.g., hydrogen and ionic bonding, π - π stacking, hydrophobic) and covalent grafting can be exploited and represent diverse options at the chemist's disposal [33].

To incorporate CPs into a silica matrix, two approaches are generally used. The first is based on the incorporation of appropriately-functionalized CP into silica by exploiting physical interactions, such as hydrogen bonding [26,30], and aromatic [34] and ionic interactions [27,35–38]. In this regard, conjugated polyelectrolytes have been widely used to take advantage of the strong ionic interactions operating between the ionic lateral chains and silanol groups. Homogeneous polythiophene/silica composite materials were also successfully prepared through the use of a poly(3-hexylthiophene) copolymer containing hydroxyl groups, due to the strong hydrogen bonding interactions with silanols [30]. More recently, covalently-linked polyfluorene-based organic-inorganic composite and hybrid materials have been reported [39,40]. By controlling either the relative amount of the silyl-functionalized monomer [39] or the degree of branching with ureasil-based silica network [40], the extent of the packing of polyfluorene chains and thus, their conformation can be controlled, allowing the promotion of the higher energy β -phase conformation.

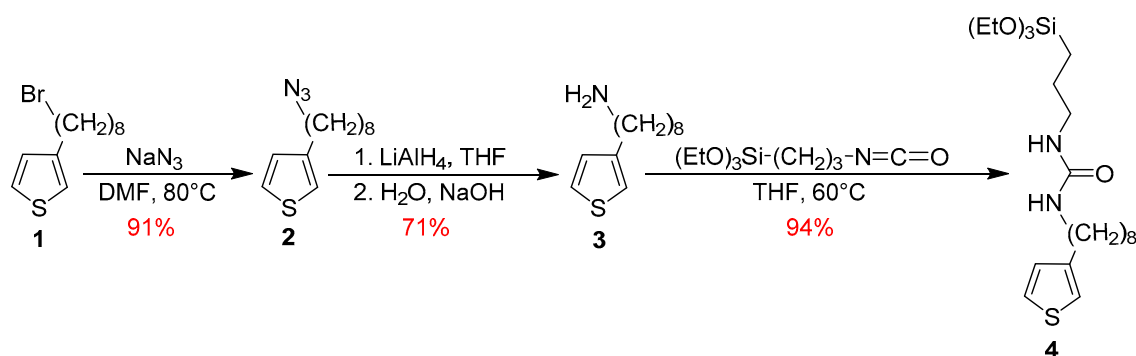
The second approach implies in situ polymerization. Here, the simplest route consists of filling silica pores with monomers and then polymerizing them. Polyaniline, polyalkyne, polythiophene, and poly(phenylene butadiynylene) have been prepared within mesoporous silica, by exploiting this strategy [41–44]. However, this approach does not guarantee a uniform pore-filling by CPs. More recently, amphiphilic molecules containing polymerizable units were designed, which serve both as a structure-directing agent, operating between the silica precursors, and the polar head groups and monomers [23,45–50], through the physical interactions (ionic interactions, hydrogen bonding). The in situ polymerization of the monomers leads to conjugated polymer chains that are uniformly distributed in the inorganic matrix. By judiciously tailoring the size of the alkyl tails or the polar head groups of the monomer-containing surfactants, the mesoscopic order of the CP/silica composite material was selectively tuned [23,45–47].

Herein, we have described the preparation of a polythiophene-silica composite material, through the self-assembly and inorganic-polymerization of a judiciously-designed thiophene-containing silylated precursor, in an acid aqueous solution, and the subsequent organic polymerization of the thiophene units. Indeed, cooperative effects originating from the hydrophobic interactions between the alkyl chains, the π -stacking interactions between the thiophene units, and the hydrogen bonding interactions between the ureido groups allow the self-assembly of silylated-thiophene precursors, and lead to ordered thiophene-silica hybrid nanostructures. In situ polymerization allows for the formation of polythiophene, within a highly ordered, inorganic environment. The formation of polythiophene was attested by the solid-state nuclear magnetic resonance (NMR) and UV-Vis spectroscopies. The absorption and emission spectra of the polythiophene-silica composite in the solid state were very similar to those reported for polythiophene, indicating no significant effect of the silica matrix on the electronic structure of polythiophene [51].

2. Results and Discussion

2.1. Synthesis of the Silylated-Thiophene Precursor

The monosilylated-thiophene monomer **4** containing a long alkyl side chain and an ureido group was synthesized according to Scheme 1.



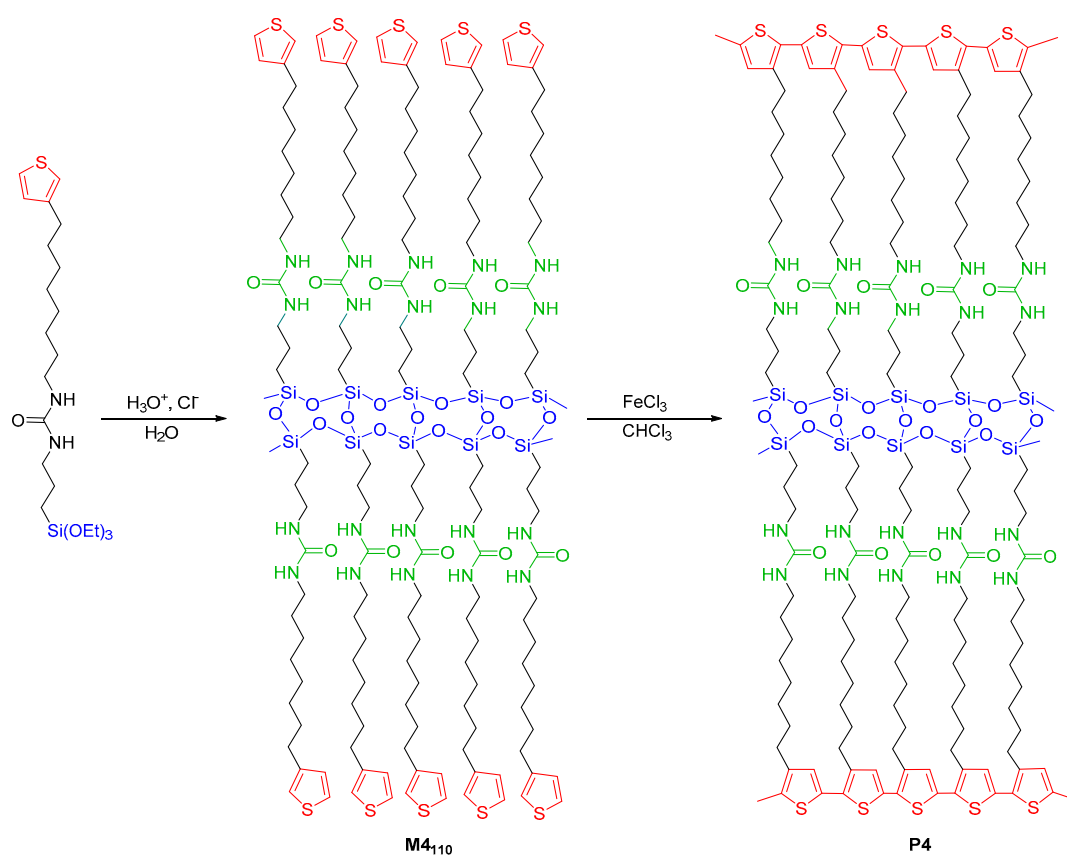
Scheme 1. Preparation of the silylated-thiophene precursor **4**.

3-(8'-Azido)thiophene (**2**) was first prepared from 3-(8'-bromooctyl)thiophene (**1**), by a nucleophilic aliphatic substitution. The presence of the azido group was evidenced by the azide antisymmetric stretching band at 2092 cm^{-1} in the IR spectrum of **2** (Figure S1 in the Supplementary Materials). The substitution of bromide by azide was also confirmed by ^1H and $^{13}\text{C}\{^1\text{H}\}$ NMR spectroscopies, with the signals at 3.25 ppm and 51.9 ppm, respectively, corresponding to CH_2N_3 (respectively, Figures S2 and S3 in the Supplementary Materials). In the second step, this compound was reduced into the corresponding amine **3** with LiAlH_4 in THF. The IR spectrum of **3** clearly indicates the presence of the asymmetrical and symmetrical N-H stretching vibrations at 3400 and 3300 cm^{-1} , characteristic of the primary amine function (Figure S4 in the Supplementary Materials). ESI-TOF mass spectrometry (positive mode) also revealed the expected $m/z = 212.1 \text{ Da}$ [$\text{M} + \text{H}^+$]. Finally, the reaction between the primary amine **3** and 3-(isocyanatopropyl)triethoxysilane quantitatively afforded the precursor **4**. Formation of **4** was confirmed by ^1H , $^{13}\text{C}\{^1\text{H}\}$, and $^{29}\text{Si}\{^1\text{H}\}$ NMR spectroscopies in CDCl_3 (respectively, Figures S7–S9 in the Supplementary Materials). The presence of the trialkoxysilyl group was attested in the ^1H -NMR spectrum of **4** by the triplet and quadruplet, at 3.78 and 1.19 ppm, respectively, which were assigned to the OCH_2 and CH_3 groups (Figure S7 in the Supplementary Materials). As expected, the $^{29}\text{Si}\{^1\text{H}\}$ spectrum of **4** exhibits only one signal at -45.2 ppm , corresponding to $\text{RSi}(\text{OEt})_3$ moieties (Figure S9 in the Supplementary Materials).

2.2. Synthesis of the Lamellar Thiophene-Silica Hybrid Material

The hydrolysis and condensation of the monosilylated precursor **4** in suspension in water at $\text{pH} = 1.5$ were first performed at room temperature for 48 h (Scheme 2). In fact, at this pH, the hydrolysis takes place while the polycondensation is induced by the self-assembly of the precursor to give the hybrid material **M4** [52].

After this time, the obtained precipitate was filtered, treated by following the usual work-up and dried (see Experimental Section). The IR spectrum of the resulting solid **M4**₂₅ revealed the presence of a very broad band at 3200 cm^{-1} , corresponding to the residual O-H bonds and indicating an incomplete polycondensation reaction (Figure S10 in the Supplementary Materials). To improve the polycondensation rate, the hybrid material **M4**₂₅ obtained previously was suspended in acidic water ($\text{pH} = 1.5$) at $110 \text{ }^\circ\text{C}$ for 24 h. Treatment of **M4**₂₅ in these conditions quantitatively afforded **M4**₁₁₀ as a white powder. The ^{29}Si CPMAS NMR spectrum of **M4**₁₁₀ showed a high rate of T^3 species (major peak around -66.0 ppm) (Figure 1). The higher degree of polycondensation for **M4**₁₁₀ was also confirmed from the results of the elemental analyses since values of C, H, N, and S content closer to theoretical ones were found.



Scheme 2. The synthetic route for the preparation of thiophene and polythiophene-based hybrid materials M4_{110} and P4 .

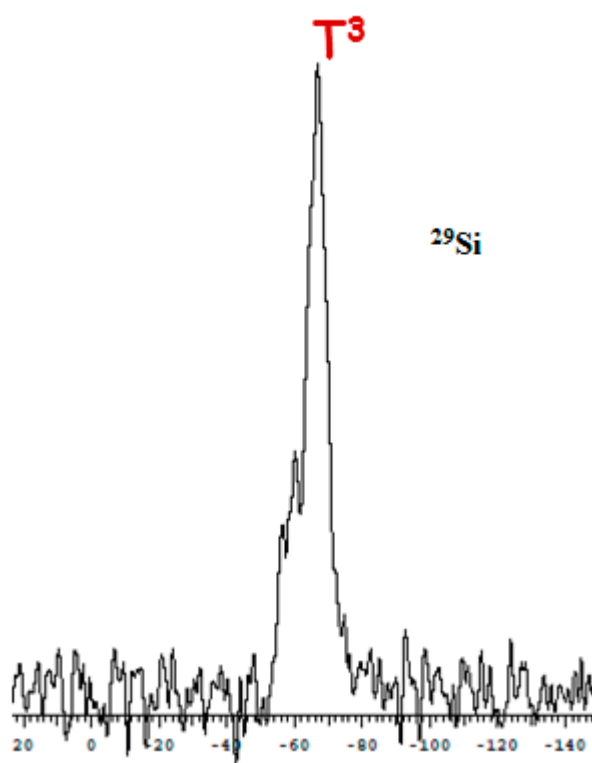


Figure 1. ^{29}Si CPMAS solid-state NMR spectrum of the hybrid material M4_{110} .

The extent of the intermolecular hydrogen bonding due to the ureido moieties was examined in **M4**₁₁₀ by FT-IR spectroscopy. Here, the differences ($\Delta\nu$) between the two vibration amide modes (amide I ($\nu_{\text{C=O}}$) and amide II (δ_{NH})) of the ureido group were used as a probe to evaluate the strength of the hydrogen bonds between the ureido groups: the lower the $\Delta\nu$ values, the stronger the hydrogen bonding interactions [53–55]. From the IR spectrum of **M4**₁₁₀, a $\Delta\nu$ of 50 cm^{-1} was calculated. This difference was of the same magnitude as the ones found for the monosilylated precursors of the formula $(\text{EtO})_3\text{Si}(\text{CH}_2)_3\text{NH}(\text{C}=\text{O})\text{NHC}_n\text{H}_{2n+1}$ ($n = 8$ and 12), and indicated significant hydrogen-bonding interactions (see Experimental section and Figure S8 in the Supplementary Materials) [55]. It was also interesting to note that no band was observed at 1680 cm^{-1} indicating no free ureido groups in this hybrid material.

The X-ray powder diffraction (XRD) pattern of **M4**₁₁₀ exhibited diffraction peaks, which are characteristic of a lamellar structure (Figure 2). Indeed, peaks at $2\theta \sim 2.86^\circ$ and 5.57° were observed, corresponding to the (100) and (200) orders with an interlayer distance of 3.1 nm (calculated using Bragg's law $n\lambda = 2d \times \sin\theta$ with $\lambda(\text{CuK}\alpha_1) = 1.542\text{ \AA}$). This value was different from the theoretical distance estimated by the ChemDraw3D calculation (3.5 nm) and corresponding to the two *N*-propyl-*N'*-(3-octylthiophene)urea units. This difference could be explained by the inclination of the alkylene chains with respect to the plane formed by the condensed siloxane units, which was not taken into account for the ChemDraw 3D calculation [56]. It is worth noting that a broad reflection, centered at $2\theta \sim 21^\circ$ was also observed, corresponding to a distance of 4.2 \AA , which is a typical value for thiophene interchain distances and also close to what can be found among siloxane units [56,57]. To determine the morphology of the hybrid material **M4**₁₁₀ on a microscopic scale, SEM analyses were performed. SEM images revealed that **M4**₁₁₀ exhibited a lamellar morphology (Figure 3, left). Further evidence for the lamellar structure was given by transmission electron microscopy (TEM) (see Figure 3, right), which displayed defined striped patterns. The thermal fragility of the material, due to a high organic content, explains the low-image resolution.

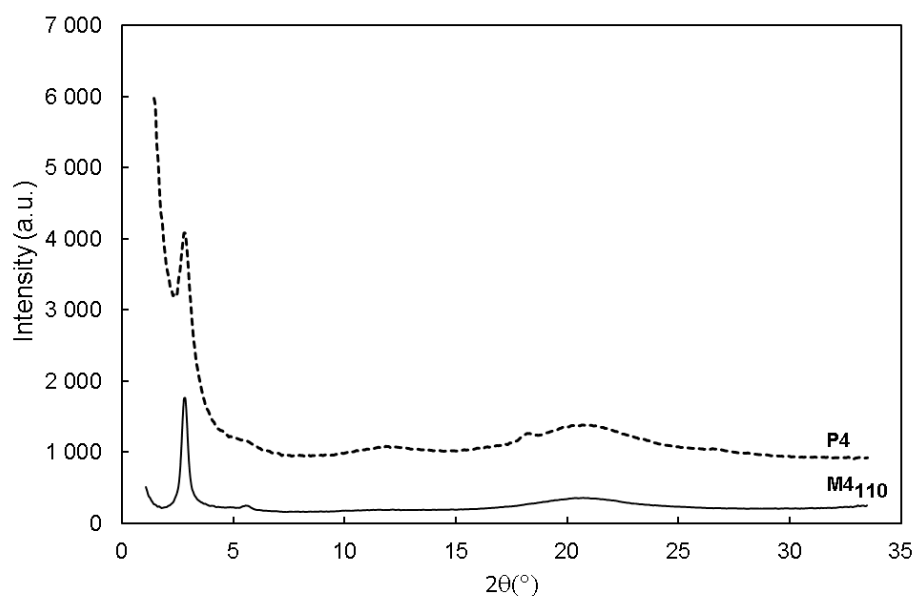


Figure 2. X-ray powder diffraction (XRD) diffractograms of thiophene-and-polythiophene-based hybrid materials **M4**₁₁₀ and **P4**.

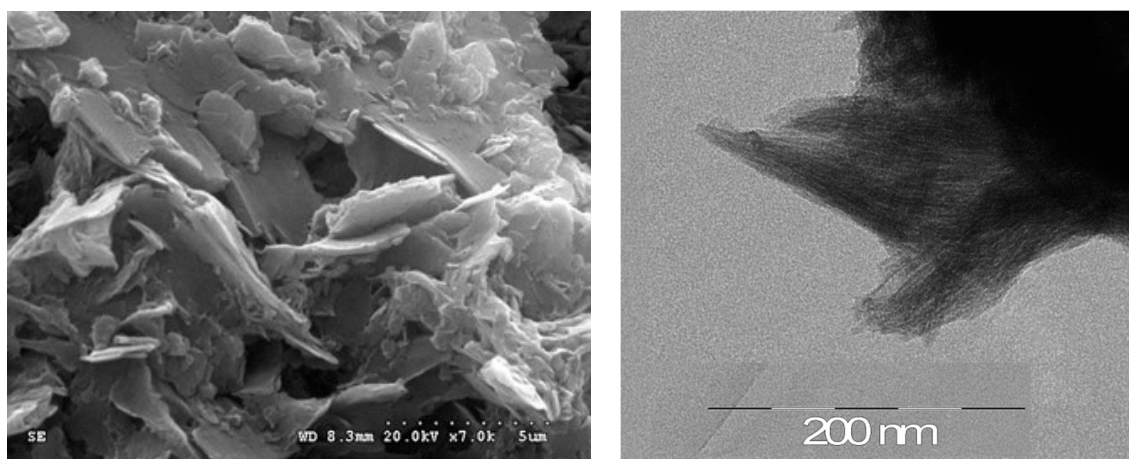


Figure 3. SEM (left) and TEM (right) images of the lamellar structure of **M4110**.

Taken together, all these data indicate that the self-assembly of the hybrid materials operated as expected, through the formation of hydrogen bonding interactions between the ureido groups, van der Waals interactions between the alkylene chains, and π - π stacking interactions between thiophene units [58]. As such, the acid hydrolysis of alkoxy silyl groups into silanol in these “pre-organized” molecular structures allowed obtaining ordered hybrid materials.

2.3. The preparation of Lamellar Polythiophene-Silica Hybrid Material

The dense packing of the thiophene groups in the interlamellar space of the hybrid materials allowed their polymerization to form the lamellar polythiophene-silica hybrid material **P4** (Scheme 2). In situ thiophene polymerization was carried out by mixing **M4110** with anhydrous FeCl_3 , a well-known thiophene polymerization oxidant [59], in chloroform, and stirring the mixture, at room temperature, for 72 h. The color of the reaction medium gradually shifted from orange (beginning of the reaction) to dark green, after 72 h (Figure S11 in the Supplementary Materials), due to the change in oxidation state of iron (III) to iron (II). After three days, the suspension was filtered and the resulting powder was thoroughly washed with water and methanol to eliminate the residual iron salts.

The hybrid material **P4** was analyzed by ^{13}C solid-state NMR, and compared to **M4110** (Figure S12 in the Supplementary Materials). After polymerization, noticeable changes were observed in the ^{13}C chemical shifts of both the aromatic and alkyl carbons, showing that their local environment was modified. Moreover, a significant broadening of the ^{13}C resonances was observed, especially for the CH_2 groups, which could be explained by a decrease in “mobility” of the alkyl chains, due to the rigidification of the material. Although the detailed assignment of the ^{13}C resonances has not been achieved so far (as it would require additional high-resolution solid-state NMR experiments), these observations strongly suggest that some interconnection between the thiophene rings had occurred. Moreover, the XRD pattern of **P4** (Figure 1) shows the preservation of the diffraction peaks, after polymerization, indicating that the lamellar structure was not affected by this polymerization process. Two additional peaks at $2\theta = 11.84^\circ$ and 18.20° , corresponding to d-spacings of 7.5 Å and 4.8 Å, respectively were noticed. These peaks might correspond to the higher-order reflection peaks of the obtained polymer [60,61]. The diffraction peak at $2\theta \sim 21^\circ$ might also indicate the persistence of the interactions between the chains in the polymer backbones [62,63]. Thermal stability of **P4** was evaluated by the thermal gravimetric analysis (TGA), from 25 °C to 600 °C, in air. The obtained curve (Figure S13 in the Supplementary Materials) showed that the hybrid material remained stable up to 180 °C and the loss of mass percentage between 180 °C and 600 °C was estimated to be around 75%, which is close to the theoretical percentage (78%).

In situ polymerization leads to a change in color from white for **M4110** to a reddish orange for **P4**, suggesting the formation of conjugated polythiophene chains. UV-vis absorption and fluorescence

spectra were recorded to investigate the optical properties of the resulting polythiophene-silica hybrid material **P4** (Figure 4). **P4** exhibited the maximum absorption and emission wavelengths, at 385 and 582 nm, respectively. Theoretical calculations and experimental measurements have shown that a linear relationship was typically observed between the adiabatic transition energy (E_{00}) and the inverse of the number of thiophene rings, allowing the determination of the effective conjugation length [64,65]. E_{00} was determined experimentally, by determining the intersection of the normalized absorption and emission spectra. Thus, by exploiting the relationship between E_{00} and the inverse of the number of thiophene units, the effective conjugation length (ECL) could be estimated. An ECL of ~ 2.9 nm, corresponding to seven substituted thiophene rings was found from the intersection of the absorption and emission spectra, at 527 nm. The length of alkyl chains at the third position of the thiophene ring, in the polymerization of the thiophene monomers, has been found to significantly influence the effective conjugation length. Indeed, long alkyl chains are more flexible and accommodating, such as dodecyl chains, and lead to a larger effective conjugation length than the shorter ones [66,67]. As such, the long alkyl chains at the third position of the thiophene ring, in **M4**₁₁₀ must have favoured effective polymerization, and thus, the conjugation length observed. This value also compares well with those previously obtained by Wang et al. for mesostructured poly(3-dodecylthiophene)-silica composite particles [46].

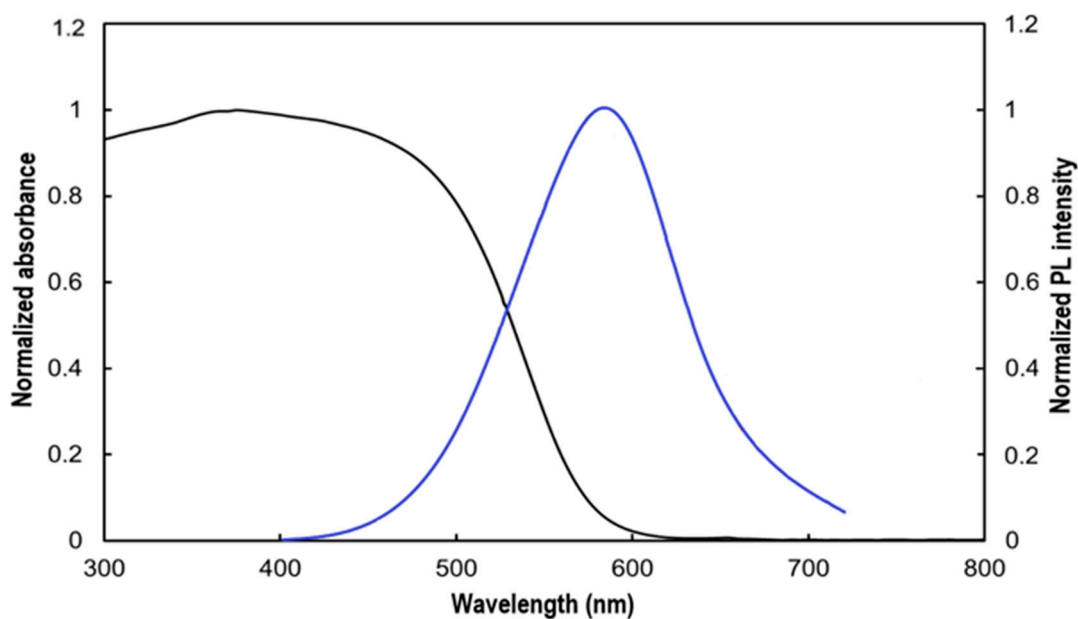


Figure 4. UV-vis absorption (black line) and fluorescence (blue line, $\lambda_{\text{exc}} = 370$ nm) spectra of the lamellar polythiophene-silica hybrid material **P4** in the solid state.

3. Experimental Method

3.1. Instrumentation and Methods

Reactions were performed under argon, using oven-dried glassware and Schlenk techniques. 3-(8'-bromooctyl)thiophene was prepared according to the literature procedure [68]. Sodium azide (99.5%), LiAlH_4 (1.0 M in THF), 3-(triethoxysilyl)propyl isocyanate (95%), anhydrous iron chloride (III) (97%) were purchased from Sigma-Aldrich (Saint Louis, MO, USA). Dry DMF and THF were obtained by using a solvent purification system, PureSolve MD5 purchased from Inert Technology (Amesbury, MA, USA). Preparative purifications were performed by silica gel flash column chromatography (Merck® 40–60 μM , Darmstadt, Germany). Solvents used as eluents were technical grade. IR spectra were recorded on a Perkin Elmer Spectrum 2 FTIR spectrophotometer (Perkin Elmer, Waltham, MA, USA). ^1H , $^{13}\text{C}\{^1\text{H}\}$ were recorded with a Bruker Avance 600 spectrometer (^1H 600.26 MHz, $^{13}\text{C}\{^1\text{H}\}$

150.96 MHz) (Bruker, Billerica, MA, USA). $^{29}\text{Si}\{^1\text{H}\}$ was acquired on a Bruker Avance 400 spectrometer (79.46 MHz) (Bruker, Billerica, MA, USA). Mass spectra (MS) were recorded on ESI-TOF Q instruments (Waters, Milford, MA, USA) in the positive mode. Elemental analyses were performed on a Vario MICRO CHNS elemental analyzer (Elementar, Langensfeld, Germany). Powder X-ray diffraction experiments were carried out on a high-resolution Bonse-Hart camera with two germanium channel cuts for very small q values (Malvern Panalytical, Worcestershire, United Kingdom). The wavelength used was 1.542 Å ($\text{CuK}\alpha$ radiation). Scanning Electron Microscopy (SEM) images were obtained with a Hitachi S2600N microscope (Hitachi, Tokyo, Japan). Transmission Electron Microscopy (TEM) observations were carried out at 100 kV (JEOL 1200 EXII) (JEOL, Tokyo, Japan). Samples for TEM measurements were prepared by embedding the hybrid material in AGAR 100 resin, followed by ultramicrotomy techniques and deposition on copper grids. The solid-state NMR spectrum for ^{29}Si was recorded on a Varian VNMRS 300 Solid spectrometer (Varian, Palo Alto, CA, USA), at a magnetic field strength of 7.05 T. A 7.5 mm MAS probe was used with a spinning rate of 5 kHz. Single pulse experiments with a continuous wave ^1H decoupling were used for ^{29}Si NMR, with 2 μs $\pi/2$ pulse duration and a recycle delay of 60 s. A recycle delay of 200 s was found necessary to allow a full ^{29}Si relaxation, although this did not lead to any change in the relative ratio of the individual components on the spectral decomposition. Thus, data with a recycle delay of 60 s could be considered as quantitative. ^{13}C solid-state NMR analyses were performed on a Varian VNMRS 600 MHz NMR spectrometer ($B_0 = 14.1$ T, $\nu_0(^1\text{H}) = 599.8$ MHz and $\nu_0(^{13}\text{C}) = 150.8$ MHz). Experiments were performed using a Varian T3 HXY 3.2 mm probe, tuned to ^1H and ^{13}C , and spinning at 18 kHz. A ^1H - ^{13}C CPMAS (Cross Polarization Magic Angle Spinning) pulse sequence was used, with a ^1H 90° excitation pulse of 2.5 μs , followed by a ramped contact pulse of 2 ms. Spinal-64 ^1H decoupling was applied during acquisition (100 kHz RF). The recycle delay was set to 1–2 s, depending on the sample, and the number of transients acquired ranged from 1430 to 7670. The ^{13}C chemical shifts were referenced to TMS (tetramethylsilane), using the deshielded resonance of adamantane (38.5 ppm) as a secondary reference.

3.2. Synthesis of 3-(8'-Azidooctyl)thiophene (2)

To a solution of 3-(6'-bromooctyl)thiophene (**1**) (6.34 g, 23.0 mmol) in DMF (100 mL) was added to sodium azide (3 g, 34.5 mmol, 1.5 eq). The mixture was stirred at 80 °C, overnight. After cooling, the mixture was diluted with CHCl_3 (75 mL) and washed three times with water (3×50 mL). The organic layer was dried over MgSO_4 and the organic solvent was removed under reduced pressure. Compound **2** was obtained as a colorless liquid (4.98 g, 91%). IR (ATR): 2092 cm^{-1} (ν_{N_3}). ^1H -NMR (CDCl_3): 7.23 (m, 1 H, H_{ar}), 6.93 (m, 2 H, 1 H_{ar}), 3.25 (t, 2 H, CH_2N_3 , $^3J_{\text{H-H}} = 6.8$ Hz), 2.63 (t, 2H, CH_2Thio , $^3J_{\text{H-H}} = 7.1$ Hz), and 1.72–1.19 (m, 12H, CH_2). $^{13}\text{C}\{^1\text{H}\}$ NMR (CDCl_3): $\delta = 143.7, 128.7, 125.5, 120.2$ (C_{ar}), 51.9 ($\text{CH}_2\text{-N}_3$), 30.9, 30.7, 29.7, 29.6, 29.2, and 27.1 (CH_2) ppm. ESI-MS: caclcd. for $[\text{C}_{12}\text{H}_{20}\text{NS}]^+$ 210.1 [M + H-N $_2$], was found to be 210.1.

3.3. Synthesis of 3-(8'-Aminooctyl)thiophene (3)

In a 250 mL two-neck round-bottom flask equipped with a refrigerant, **2** (4.74 g, 20.0 mmol) was dissolved in THF (40 mL). After cooling to 0 °C, LiAlH_4 (40 mL, 40.0 mmol, 1.0 M solution in THF) was added in drops. After the reaction was judged complete by TLC (eluent: *n*-pentane/ CH_2Cl_2 1/1), the reaction was quenched with 15% aqueous NaOH (1.6 mL), then followed by ice water (3×1.6 mL). The precipitated aluminum salts were filtered. The filtrate was dried with anhydrous MgSO_4 and the solvent was removed by evaporation. Compound **3** was obtained as a colorless liquid (4.98 g, 71 %). IR (ATR): 3400, 3300 cm^{-1} (ν_{NH_2}). ^1H -NMR (CDCl_3): $\delta = 7.23$ ppm (s, 1H, Th), 6.93 (m, 2H, Th), 2.68 (t, 2H, $\text{CH}_2\text{-Th}$, $^3J_{\text{H-H}} = 7.5$ Hz), 2.62 (t, 2H, $\text{CH}_2\text{-NH}_2$, $^3J_{\text{H-H}} = 6.7$ Hz), and 1.74–1.15 (m, 12H, CH_2) ppm. $^{13}\text{C}\{^1\text{H}\}$ NMR (CDCl_3): $\delta = 143.0, 128.7, 125.5, 120.2$ (Th), 51.9 ($\text{CH}_2\text{-N}$), 30.9, 30.6, 29.7, 29.6, 29.5, 29.2, and 27.1 (CH_2) ppm. ESI-MS: caclcd. for $[\text{C}_{12}\text{H}_{22}\text{NS}]^+$ 212.1 [M + H], was found to be 212.1.

3.4. Synthesis of the Thiophene Silylated Precursor (4)

To a solution of **3** (2.89 g, 14.0 mmol) in THF (35 mL), 3-isocyanatopropyltriethoxysilane (3.8 mL, 15.0 mmol) was slowly added under stirring and the reaction was heated, at 60 °C for 2 h. THF was evaporated under reduced pressure to obtain a viscous oil and *n*-pentane (50 mL) was then added to precipitate **4**. The liquid supernatant containing the excess of 3-isocyanatopropyltriethoxysilane was removed and the precipitate was washed three more times with *n*-pentane (25 mL). The compound **4** was then dried under vacuum and obtained as a white solid in 94% yield (6.03 g). IR (ATR): 3312 cm⁻¹ (νNH), 1628 cm⁻¹ (νCO_{amide}). ¹H-NMR (CDCl₃): δ = 7.19 (m, 1H, Th), 6.88 (m, 2H, Th), 5.20–4.86 (m, 2H, NH-CO-NH), 3.78 (q, 6H, O-CH₂, ³J_{H-H} = 7.0 Hz), 3.09 (m, 4H, CH₂-N), 2.58 (t, 2H, CH₂, ³J_{H-H} = 7.3 Hz), 1.24–1.68 (m, 14H, CH₂), 1.19 (t, 9H, CH₃, ³J_{H-H} = 7.0 Hz), and 0.60 (t, 2H, CH₂-Si, ³J_{H-H} = 8.1 Hz) ppm. ¹³C{¹H} NMR (CDCl₃): δ = 158.9 (CO), 143.1, 128.3, 125.1, 119.8 (Th), 58.4, 42.9, 40.5, 30.6, 30.4, 30.3, 29.5, 29.4, 29.3, 27.0, 23.7, 18.3, and 7.8 ppm. ²⁹Si{¹H} NMR (CDCl₃) δ = -45.2 ppm. Anal. calcd. for C₂₂H₄₂N₂O₄SSi (458.26): %C 57.60, %H 9.23; %N 6.11, %S 6.99 was found to be %C 57.76, %H 9.04; %N 5.98, and %S 6.90.

3.5. Synthesis of the Lamellar Thiophene-silica Hybrid Materials

Compound **4** (4.58 g, 10.0 mmol) was placed into a Schlenk tube with acidified water (30 mL, pH = 1.5) and stirred, at room temperature for 48 h. The resulting solid was filtered and dried under vacuum, leading to material **M4**₂₅. Half of this solid was then placed into a Schlenk tube and 30 mL of water, at pH = 1.5 was added. The resulting solution was stirred at 110 °C for 24 h. After cooling, the white precipitate was isolated by filtration, washed three times with water and then dried under vacuum leading to material **M4**₁₁₀.

M4₂₅: IR (ATR): ν = 3311 (νNH stretching), 3200 (νOH stretching), 2926, 2845 (νCH₂), 1626 (νC=O stretching), and 1572 (δNH bending) cm⁻¹. Anal. calcd. for C₁₆H₂₇N₂O_{2.5}SSi (347.15): %C 55.29, %H 7.83; %N 8.06, %S 9.22 was found to be %C 40.30, %H 6.97; %N 5.93, and %S 6.60.

M4₁₁₀: IR (ATR): ν = 3318 (νNH stretching), 2924, 2852 (νCH₂), 1622 (νC=O stretching), and 1572 (δNH bending) cm⁻¹. Anal. calcd for C₁₆H₂₇N₂O_{2.5}SSi (347.15): %C 55.29, %H 7.83; %N 8.06, %S 9.22 was found to be %C 53.57, %H 8.97; %N 7.89, and %S 9.16.

3.6. In Situ Polymerization of Thiophene Groups

Anhydrous iron chloride (III) (0.8 g) and dried chloroform (10 mL) were placed in a round-bottom flask under inert atmosphere. Thiophene-silica composite material (0.3 g) was added and the resulting mixture was stirred, at room temperature for 72 h. The suspension was then filtered and washed with water (2 × 10 mL) and methanol (2 × 10 mL) by centrifugation, and dried under vacuum leading to an orange-red solid.

4. Conclusions

A new layered polythiophene-silica hybrid material was prepared by hydrolysis and polycondensation of a judiciously-designed, monosilylated-thiophene precursor and its subsequent polymerization. By exploiting the self-assembly of this silylated-thiophene precursor, through van der Waals interactions of alkylene chains, π-stacking interactions between the thiophene units, and hydrogen bonding interactions between ureido groups, a lamellar thiophene-silica hybrid material was achieved. Then, the dense packing of thiophene groups in the central region of the lamellar silica structure allowed the in situ polymerization to form an ordered polythiophene-silica composite. The formation of nanostructured polythiophene-silica was confirmed by combining XRD, TEM, solid-state NMR, and UV-Vis absorption spectroscopy. The UV-Vis absorption and emission spectra of the polythiophene-silica composite in the solid state were very similar to those reported for polythiophene, indicating no significant effect of the silica matrix on the electronic structure of polythiophene. We believe that our strategy represents an efficient approach towards the formation

of nanostructured, conjugated, polymers-based hybrid materials with tunable properties, through a judicious design of the silylated monomer.

Supplementary Materials: The following are available online at <http://www.mdpi.com/1420-3049/23/10/2510/s1>, Figure S1: ATR-FT-IR spectrum of **2**, Figure S2: ^1H -NMR spectrum of **2** in CDCl_3 , Figure S3: $^{13}\text{C}\{^1\text{H}\}$ NMR spectrum of **2** in CDCl_3 , Figure S4: ATR-FT-IR spectrum of **3**, Figure S5: ^1H -NMR spectrum of **3** in CDCl_3 , Figure S6: $^{13}\text{C}\{^1\text{H}\}$ NMR spectrum of **3** in CDCl_3 , Figure S7: ^1H -NMR spectrum of **4** in CDCl_3 , Figure S8: $^{13}\text{C}\{^1\text{H}\}$ NMR spectrum of **4** in CDCl_3 , Figure S9: $^{29}\text{Si}\{^1\text{H}\}$ NMR spectrum of **4** in CDCl_3 , Figure S10: IR spectra of hybrid materials **M4**₂₅ (bottom) and **M4**₁₁₀ (top), Figure S11: Color evolution during the chemical polymerization of thiophene units in **M4**₁₁₀. Figure S12: ^{13}C -CPMAS solid-state NMR spectra of **M4**₁₁₀ and **P4**. Figure S13: TGA curve of lamellar polythiophene-silica hybrid material **P4**.

Author Contributions: M.-J.Z. carried out the synthesis of the thiophene and polythiophene-silica hybrid materials. D.L. performed the characterization of the hybrid materials by ^{13}C solid-state NMR. S.R. performed the UV/Vis absorption and photoluminescence experiments. A.M. and S.C. conceived the idea, supervised the research and wrote the paper.

Funding: This research received no external funding.

Acknowledgments: The authors are grateful to the University of Montpellier, the CNRS and the French Ministry of Research for financial support.

Conflicts of Interest: The authors declare no conflict of interest.

References

1. Wu, J.-S.; Cheng, S.-W.; Cheng, Y.-J.; Hsu, C.-S. Donor-acceptor conjugated polymers based on multifused ladder-type arenes for organic solar cells. *Chem. Soc. Rev.* **2015**, *44*, 1113–1154. [[CrossRef](#)] [[PubMed](#)]
2. Richard, H.; Anna, K.; Peter, M.-B.; Fabian, P.; Mukundan, T. π -conjugated donor polymers: Structure formation and morphology in solution, bulk and photovoltaic blends. *Adv. Energy Mater.* **2017**, *7*, 1700314. [[CrossRef](#)]
3. Kang, H.; Lee, W.; Oh, J.; Kim, T.; Lee, C.; Kim, B.J. From fullerene-polymer to all-polymer solar cells: The importance of molecular packing, orientation, and morphology control. *Acc. Chem. Res.* **2016**, *49*, 2424–2434. [[CrossRef](#)] [[PubMed](#)]
4. Chou, Y.-H.; Chang, H.-C.; Liu, C.-L.; Chen, W.-C. Polymeric charge storage electrets for non-volatile organic field effect transistor memory devices. *Polym. Chem.* **2015**, *6*, 341–352. [[CrossRef](#)]
5. Henning, S. Organic Field-Effect Transistors: The path beyond amorphous silicon. *Adv. Mater.* **2014**, *26*, 1319–1335. [[CrossRef](#)]
6. Facchetti, A. Semiconductors for organic transistors. *Mater. Today* **2007**, *10*, 28–37. [[CrossRef](#)]
7. Lei, Y.; Cheuk-Lam, H.; Hongbin, W.; Yong, C.; Wai-Yeung, W. White polymer light-emitting devices for solid-state lighting: Materials, devices, and recent progress. *Adv. Mater.* **2014**, *26*, 2459–2473. [[CrossRef](#)]
8. Dai, L.; Winkler, B.; Dong, L.; Tong, L.; Mau, A.W.H. Conjugated Polymers for Light-Emitting Applications. *Adv. Mater.* **2001**, *13*, 915–925. [[CrossRef](#)]
9. Xie, J.; Zhao, C.; Lin, Z.-Q.; Gu, P.-Y.; Zhang, Q. Nanostructured Conjugated Polymers for Energy-Related Applications beyond Solar Cells. *Chem. Asian J.* **2016**, *11*, 1489–1511. [[CrossRef](#)] [[PubMed](#)]
10. Xie, J.; Gu, P.; Zhang, Q. Nanostructured Conjugated Polymers: Toward High-Performance Organic Electrodes for Rechargeable Batteries. *ACS Energy Lett.* **2017**, *2*, 1985–1996. [[CrossRef](#)]
11. Wang, J.; Lv, F.; Liu, L.; Ma, Y.; Wang, S. Strategies to design conjugated polymer based materials for biological sensing and imaging. *Coord. Chem. Rev.* **2018**, *354*, 135–154. [[CrossRef](#)]
12. Liang, J.; Li, K.; Liu, B. Visual sensing with conjugated polyelectrolytes. *Chem. Sci.* **2013**, *4*, 1377–1394. [[CrossRef](#)]
13. Park, J.; Lee, C.; Jung, J.; Kang, H.; Kim, K.-H.; Ma, B.; Kim, B.J. Facile photo-crosslinking of azide-containing hole-transporting polymers for highly efficient, solution-processed, multilayer organic light emitting devices. *Adv. Funct. Mater.* **2014**, *24*, 7588–7596. [[CrossRef](#)]
14. Trattinig, R.; Pevzner, L.; Jäger, M.; Schlesinger, R.; Nardi, M.V.; Ligorio, G.; Christodoulou, C.; Koch, N.; Baumgarten, M.; Müllen, K.; et al. Bright blue solution processed triple-layer polymer light-emitting diodes realized by thermal layer stabilization and orthogonal solvents. *Adv. Funct. Mater.* **2013**, *23*, 4897–4905. [[CrossRef](#)]

15. Maturová, K.; van Bavel Svetlana, S.; Wienk Martijn, M.; Janssen, R.A.J.; Kemerink, M. Description of the morphology dependent charge transport and performance of polymer: Fullerene bulk heterojunction solar cells. *Adv. Funct. Mater.* **2010**, *21*, 261–269. [[CrossRef](#)]
16. Li, G.; Shrotriya, V.; Huang, J.; Yao, Y.; Moriarty, T.; Emery, K.; Yang, Y. High-efficiency solution processable polymer photovoltaic cells by self-organization of polymer blends. *Nat. Mater.* **2005**, *4*, 80–84. [[CrossRef](#)]
17. Ruderer, M.A.; Muller-Buschbaum, P. Morphology of polymer-based bulk heterojunction films for organic photovoltaics. *Soft Matter* **2011**, *7*, 5482–5493. [[CrossRef](#)]
18. Kim, Y.; Cook, S.; Tuladhar, S.M.; Choulis, S.A.; Nelson, J.; Durrant, J.R.; Bradley, D.D.C.; Giles, M.; McCulloch, I.; Ha, C.-S.; et al. A strong regioregularity effect in self-organizing conjugated polymer films and high-efficiency polythiophene:fullerene solar cells. *Nat. Mater.* **2006**, *5*, 63–69. [[CrossRef](#)]
19. Sirringhaus, H.; Brown, P.J.; Friend, R.H.; Nielsen, M.M.; Bechgaard, K.; Langeveld-Voss, B.M.W.; Spiering, A.J.H.; Janssen, R.A.J.; Meijer, E.W.; Herwig, P.; et al. Two-dimensional charge transport in self-organized, high-mobility conjugated polymers. *Nature* **1999**, *401*, 685–688. [[CrossRef](#)]
20. Beljonne, D.; Pourtois, G.; Silva, C.; Hennebicq, E.; Herz, L.M.; Friend, R.H.; Scholes, G.D.; Setayesh, S.; Müllen, K.; Brédas, J.L. Interchain vs. intrachain energy transfer in acceptor-capped conjugated polymers. *Proc. Natl. Acad. Sci. USA* **2002**, *99*, 10982–10987. [[CrossRef](#)] [[PubMed](#)]
21. Rivaton, A.; Tournebize, A.; Gaume, J.; Bussièrre, P.-O.; Gardette, J.-L.; Therias, S. Photostability of organic materials used in polymer solar cells. *Polym. Int.* **2013**, *63*, 1335–1345. [[CrossRef](#)]
22. Manceau, M.; Rivaton, A.; Gardette, J.-L.; Guillerez, S.; Lemaître, N. The mechanism of photo- and thermooxidation of poly(3-hexylthiophene) (P3HT) reconsidered. *Polym. Degrad. Stab.* **2009**, *94*, 898–907. [[CrossRef](#)]
23. Yang, B.; Xiao, M.; Zhao, C.; Zhang, S.; Jiang, A.; Wang, J. Alignment control of polythiophene chains with mesostructured silica nanofibers having different pore orientations. *Small* **2012**, *8*, 2021–2026. [[CrossRef](#)]
24. Evans, R.C.; Marr, P.C. Chain confinement promotes β -phase formation in polyfluorene-based photoluminescent ionogels. *Chem. Commun.* **2012**, *48*, 3742–3744. [[CrossRef](#)] [[PubMed](#)]
25. Cheminet, N.; Jarrosson, T.; Lere-Porte, J.-P.; Serein-Spirau, F.; Cury, L.; Moreau, J.; Viau, L.; Vioux, A. One pot synthesis of fluorescent π -conjugated materials: Immobilization of phenylene-ethynylene polyelectrolytes in silica confined ionogels. *J. Mater. Chem.* **2011**, *21*, 13588–13593. [[CrossRef](#)]
26. Ayumi, M.; Yuta, M.; Takahiro, U.; Takahito, I.; Takayuki, Y.; Akira, K.; Masataka, K. Incorporation of fluorene-based emitting polymers into silica. *J. Polym. Sci. Part A Polym. Chem.* **2010**, *48*, 5322–5328. [[CrossRef](#)]
27. Evans, R.C.; Macedo, A.G.; Pradhan, S.; Scherf, U.; Carlos, L.D.; Burrows, H.D. Fluorene based conjugated polyelectrolyte/silica nanocomposites: Charge-mediated phase aggregation at the organic-inorganic interface. *Adv. Mater.* **2010**, *22*, 3032–3037. [[CrossRef](#)] [[PubMed](#)]
28. Aharon, E.; Kalina, M.; Frey, G.L. Inhibition of energy transfer between conjugated polymer chains in host/guest nanocomposites generates white photo- and electroluminescence. *J. Am. Chem. Soc.* **2006**, *128*, 15968–15969. [[CrossRef](#)] [[PubMed](#)]
29. Kelly, T.L.; Yamada, Y.; Schneider, C.; Yano, K.; Wolf, M.O. Enhanced optical properties and opaline self-assembly of ppv encapsulated in mesoporous silica spheres. *Adv. Funct. Mater.* **2009**, *19*, 3737–3745. [[CrossRef](#)]
30. Kubo, M.; Takimoto, C.; Minami, Y.; Uno, T.; Itoh, T.; Shoyama, M. Incorporation of π -conjugated polymer into silica: preparation of poly[2-methoxy-5-(2-ethylhexyloxy)-1,4-phenylenevinylene]/silica and poly(3-hexylthiophene)/silica composites. *Macromolecules* **2005**, *38*, 7314–7320. [[CrossRef](#)]
31. Rothberg, L.J.; Yan, M.; Papadimitrakopoulos, F.; Galvin, M.E.; Kwock, E.W.; Miller, T.M. Photophysics of phenylenevinylene polymers. *Synth. Met.* **1996**, *80*, 41–58. [[CrossRef](#)]
32. Jakubiak, R.; Collison, C.J.; Wan, W.C.; Rothberg, L.J.; Hsieh, B.R. Aggregation quenching of luminescence in electroluminescent conjugated polymers. *J. Phys. Chem. A* **1999**, *103*, 2394–2398. [[CrossRef](#)]
33. Evans, R.C. Harnessing self-assembly strategies for the rational design of conjugated polymer based materials. *J. Mater. Chem. C* **2013**, *1*, 4190–4200. [[CrossRef](#)]
34. Tamaki, R.; Samura, K.; Chujo, Y. Synthesis of polystyrene and silica gel polymer hybrids via π - π interactions. *Chem. Commun.* **1998**, 1131–1132. [[CrossRef](#)]
35. Ogoshi, T.; Chujo, Y. Synthesis of amorphous and nanostructured cationic polyacetylene/silica hybrids by using ionic interactions. *Macromolecules* **2005**, *38*, 9110–9116. [[CrossRef](#)]

36. Clement, S.; Tizit, A.; Desbief, S.; Mehdi, A.; De Winter, J.; Gerbaux, P.; Lazzaroni, R.; Boury, B. Synthesis and characterisation of π -conjugated polymer/silica hybrids containing regioregular ionic polythiophenes. *J. Mater. Chem.* **2011**, *21*, 2733–2739. [[CrossRef](#)]
37. Willis-Fox, N.; Kraft, M.; Arlt, J.; Scherf, U.; Evans, R.C. Tunable white-light emission from conjugated polymer-di-ureasil materials. *Adv. Funct. Mater.* **2016**, *26*, 532–542. [[CrossRef](#)]
38. Willis-Fox, N.; Marques, A.-T.; Arlt, J.; Scherf, U.; Carlos, L.D.; Burrows, H.D.; Evans, R.C. Synergistic photoluminescence enhancement in conjugated polymer-di-ureasil organic-inorganic composites. *Chem. Sci.* **2015**, *6*, 7227–7237. [[CrossRef](#)] [[PubMed](#)]
39. Behrendt, J.M.; Foster, A.B.; McCairn, M.C.; Willcock, H.; O'Reilly, R.K.; Turner, M.L. Hybrid inorganic-organic composite nanoparticles from crosslinkable polyfluorenes. *J. Mater. Chem. C* **2013**, *1*, 3297–3304. [[CrossRef](#)]
40. Meazzini, I.; Behrendt, J.M.; Turner, M.L.; Evans, R.C. Targeted β -phase formation in poly(fluorene)-ureasil grafted organic-inorganic hybrids. *Macromolecules* **2017**, *50*, 4235–4243. [[CrossRef](#)]
41. Wu, C.-G.; Bein, T. Conducting polyaniline filaments in a mesoporous channel host. *Science* **1994**, *264*, 1757–1759. [[CrossRef](#)] [[PubMed](#)]
42. Kelly, T.L.; Che, S.P.Y.; Yamada, Y.; Yano, K.; Wolf, M.O. Influence of surface morphology on the colloidal and electronic behavior of conjugated polymer-silica microspheres. *Langmuir* **2008**, *24*, 9809–9815. [[CrossRef](#)] [[PubMed](#)]
43. Lin, V.S.Y.; Radu, D.R.; Han, M.-K.; Deng, W.; Kuroki, S.; Shanks, B.H.; Pruski, M. Oxidative polymerization of 1,4-diethynylbenzene into highly conjugated poly(phenylene butadiynylene) within the channels of surface-functionalized mesoporous silica and alumina materials. *J. Am. Chem. Soc.* **2002**, *124*, 9040–9041. [[CrossRef](#)] [[PubMed](#)]
44. Cardin, D.J.; Constantine, S.P.; Gilbert, A.; Lay, A.K.; Alvaro, M.; Galletero, M.S.; Garcia, H.; Marquez, F. Polymerization of alkynes in the channels of mesoporous materials containing Ni and Zn cations: Almost complete filling of the voids. *J. Am. Chem. Soc.* **2001**, *123*, 3141–3142. [[CrossRef](#)]
45. Yang, Y.; Lu, Y.; Lu, M.; Huang, J.; Haddad, R.; Xomeritakis, G.; Liu, N.; Malanoski, A.P.; Sturmayer, D.; Fan, H.; et al. Functional nanocomposites prepared by self-assembly and polymerization of diacetylene surfactants and silicic acid. *J. Am. Chem. Soc.* **2003**, *125*, 1269–1277. [[CrossRef](#)] [[PubMed](#)]
46. Yang, Z.; Kou, X.; Ni, W.; Sun, Z.; Li, L.; Wang, J. Fluorescent mesostructured polythiophene-silica composite particles synthesized by in situ polymerization of structure-directing monomers. *Chem. Mater.* **2007**, *19*, 6222–6229. [[CrossRef](#)]
47. Lu, Y.; Yang, Y.; Sellinger, A.; Lu, M.; Huang, J.; Fan, H.; Haddad, R.; Lopez, G.; Burns, A.R.; Sasaki, D.Y.; et al. Self-assembly of mesoscopically ordered chromatic polydiacetylene/silica nanocomposites. *Nature* **2001**, *410*, 913–917. [[CrossRef](#)] [[PubMed](#)]
48. Takuzo, A.; Keisuke, T. Photoluminescent silicate microsticks containing aligned nanodomains of conjugated polymers by sol-gel-based in situ polymerization. *Angew. Chem. Int. Ed.* **2001**, *40*, 3803–3806. [[CrossRef](#)]
49. Guangtao, L.; Sheshanath, B.; Tianyu, W.; Yang, Z.; Hesun, Z.; Jürgen-Hinrich, F. Gram-scale synthesis of submicrometer-long polythiophene wires in mesoporous silica matrices. *Angew. Chem. Int. Ed.* **2003**, *42*, 3818–3821. [[CrossRef](#)]
50. Peng, H.; Tang, J.; Yang, L.; Pang, J.; Ashbaugh, H.S.; Brinker, C.J.; Yang, Z.; Lu, Y. Responsive periodic mesoporous polydiacetylene/silica nanocomposites. *J. Am. Chem. Soc.* **2006**, *128*, 5304–5305. [[CrossRef](#)] [[PubMed](#)]
51. Roncali, J. Conjugated poly(thiophenes): Synthesis, functionalization, and applications. *Chem. Rev.* **1992**, *92*, 711–738. [[CrossRef](#)]
52. Mouawia, R.; Mehdi, A.; Reyé, C.; Corriu, R.J.P. From simple molecules to highly functionalised lamellar materials. *J. Mater. Chem.* **2008**, *18*, 2028–2035. [[CrossRef](#)]
53. Moreau, J.J.E.; Vellutini, L.; Wong Chi Man, M.; Bied, C.; Dieudonné, P.; Bantignies, J.-L.; Sauvajol, J.-L. Lamellar bridged silsesquioxanes: Self-assembly through a combination of hydrogen bonding and hydrophobic interactions. *Chem. Eur. J.* **2005**, *11*, 1527–1537. [[CrossRef](#)] [[PubMed](#)]
54. van Esch, J.H.; Schoonbeek, F.; de Loos, M.; Kooijman, H.; Spek, A.L.; Kellogg, R.M.; Feringa, B.L. Cyclic bis-urea compounds as gelators for organic solvents. *Chem. Eur. J.* **1999**, *5*, 937–950. [[CrossRef](#)]
55. Besson, E.; Mehdi, A.; Reyé, C.; Gaveau, P.; Corriu, R.J.P. Self-assembly of layered organosilicas based on weak intermolecular interactions. *Dalton Trans.* **2010**, *39*, 7534–7539. [[CrossRef](#)] [[PubMed](#)]

56. Besson, E.; Mehdi, A.; Van der Lee, A.; Chollet, H.; Reyé, C.; Guillard, R.; Corriu, R.J.P. Selective lanthanides sequestration based on a self-assembled organosilica. *Chem. Eur. J.* **2010**, *16*, 10226–10233. [[CrossRef](#)] [[PubMed](#)]
57. Tsuzuki, S.; Honda, K.; Azumi, R. Model chemistry calculations of thiophene dimer interactions: Origin of π -stacking. *J. Am. Chem. Soc.* **2002**, *124*, 12200–12209. [[CrossRef](#)] [[PubMed](#)]
58. Alauzun, J.; Mehdi, A.; Reyé, C.; Corriu, R.J.P. Hydrophilic conditions: A new way for self-assembly of hybrid silica containing long alkylene chains. *J. Mater. Chem.* **2005**, *15*, 841–843. [[CrossRef](#)]
59. Niemi, V.M.; Knuuttila, P.; Österholm, J.E.; Korvola, J. Polymerization of 3-alkylthiophenes with FeCl_3 . *Polymer* **1992**, *33*, 1559–1562. [[CrossRef](#)]
60. Qiao, X.; Wang, X.; Mo, Z. The effects of different alkyl substitution on the structures and properties of poly(3-alkylthiophenes). *Synth. Met.* **2001**, *118*, 89–95. [[CrossRef](#)]
61. Łuzny, W.; Trznadel, M.; Proń, A. X-ray diffraction study of regioregular poly(3-alkylthiophenes). *Synth. Met.* **1996**, *81*, 71–74. [[CrossRef](#)]
62. Hundt, N.; Hoang, Q.; Nguyen, H.; Sista, P.; Hao, J.; Servello, J.; Palaniappan, K.; Alemseghed, M.; Biewer, M.C.; Stefan, M.C. Synthesis and Characterization of a Block Copolymer Containing Regioregular Poly(3-hexylthiophene) and Poly(γ -benzyl-L-glutamate). *Macromol. Rapid Commun.* **2011**, *32*, 302–308. [[CrossRef](#)] [[PubMed](#)]
63. Bhatt, M.P.; Sista, P.; Hao, J.; Hundt, N.; Biewer, M.C.; Stefan, M.C. Electronic properties-morphology correlation of a rod-rod semiconducting liquid crystalline block copolymer containing poly(3-hexylthiophene). *Langmuir* **2012**, *28*, 12762–12770. [[CrossRef](#)] [[PubMed](#)]
64. Peter, B. End-capped oligothiophenes-new model compounds for polythiophenes. *Adv. Mater.* **1992**, *4*, 102–107. [[CrossRef](#)]
65. Gierschner, J.; Cornil, J.; Egelhaaf, H.-J. Optical bandgaps of π -conjugated organic materials at the polymer limit: Experiment and theory. *Adv. Mater.* **2007**, *19*, 173–191. [[CrossRef](#)]
66. Chen, S.-A.; Ni, J.-M. Facile Structure/properties of conjugated conductive polymers. 1. Neutral poly(3-alkylthiophene)s. *Macromolecules* **1992**, *25*, 6081–6089. [[CrossRef](#)]
67. Ho, K.-S.; Bartus, J.; Levon, K.; Mao, J.; Zheng, W.-Y.; Laakso, J.; Taka, T. Layered structure with side chain crystallinity in undoped poly(3-alkyl thiophenes). *Synth. Met.* **1993**, *55*, 384–387. [[CrossRef](#)]
68. Peter, B.; Frank, W.; Stephan, H. Facile synthesis of 3-(ω -haloalkyl)thiophenes as key building blocks for functionalized thiophenes and polythiophenes. *Angew. Chem. Int. Ed. Engl.* **1990**, *29*, 419–420. [[CrossRef](#)]

Sample Availability: Samples of the compounds described in this manuscript are not available from the authors.



© 2018 by the authors. Licensee MDPI, Basel, Switzerland. This article is an open access article distributed under the terms and conditions of the Creative Commons Attribution (CC BY) license (<http://creativecommons.org/licenses/by/4.0/>).